

Received 20 August 2022, accepted 11 October 2022, date of publication 19 October 2022, date of current version 26 October 2022.

Digital Object Identifier 10.1109/ACCESS.2022.3215434



## RESEARCH ARTICLE

# Microgrid Power Sharing Framework for Software Defined Networking and Cybersecurity Analysis

RICARDO E. PÉREZ GUZMÁN<sup>ID1</sup>, (Member, IEEE),

MARCO RIVERA<sup>ID2</sup>, (Senior Member, IEEE), PATRICK W. WHEELER<sup>ID3</sup>, (Fellow, IEEE),

GALINA MIRZAEVA<sup>ID4</sup>, (Senior Member, IEEE), EDUARDO E. ESPINOSA<sup>ID5</sup>, (Member, IEEE),

AND JAIME A. ROHLEN<sup>ID6</sup>, (Senior Member, IEEE)

<sup>1</sup>Department of Computer Science, Faculty of Engineering, Universidad de Talca, Curicó 3460000, Chile

<sup>2</sup>Technological Center for Energy Conversion, Faculty of Engineering, Universidad de Talca, Curicó 3460000, Chile

<sup>3</sup>Department of Electrical and Electronic Engineering, Faculty of Science and Engineering, University of Nottingham, NG7 2RD Nottingham, U.K.

<sup>4</sup>School of Electrical Engineering and Computer Science, University of Newcastle, Callaghan, NSW 2308, Australia

<sup>5</sup>Department of Electrical Engineering, Engineering Faculty, Universidad Católica de la Santísima Concepción, Concepción 4090541, Chile

<sup>6</sup>Department of Electrical and Electronic Engineering, Universidad del Bío-Bío, Concepción 4051381, Chile

Corresponding author: Marco Rivera (marcoriv@utalca.cl)

This work was supported in part by the National Doctorate Scholarship Agencia Nacional de Investigación y Desarrollo (ANID) 2019, in part by the Fondo Nacional de Desarrollo Científico y Tecnológico (FONDECYT) Regular Research under Project 1220556, in part by the Fondo de Financiamiento de Centros de Investigación en Áreas Prioritarias (FONDAP) Solar Energy Research Center (SERC) Chile under Grant 15110019, in part by the ANID Climat AMSUD210001, in part by the Dirección de Investigación of Universidad de Talca, and in part by the Project MEC80190074.

**ABSTRACT** Hierarchical control is a widely used strategy that can increase resilience and improve the reliability of the electrical network based on microgrid global variables. The large amounts of data required during transitions prompt the use of more reliable and flexible communications to achieve the control objectives. Such communications can involve potential cyber vulnerabilities and latency restrictions, which cannot be always addressed in real-time. To accurately capture the system's overall operation, this paper proposes a co-simulation framework driven by flexible communications and a resilient control algorithm to regulate the frequency and voltage deviations in a networked microgrid. Model-based predictive control has been implemented, to avoid slow transient response associated with linear hierarchical control. Software-Defined Networking (SDN) is responsible for increasing the communication intelligence during the power-sharing process. The effects of critical communications and overall system performance are reviewed and compared for different co-simulation scenarios. Graphical Network Simulator (GNS3) is used in combination with model-based predictive control and SDN, to provide latency below 100 ms, as defined in IEC 61850. Testing of the proposed system under different cyber attack scenarios demonstrate its excellent performance. The novel control architecture presented in the paper provides a reference framework for future cloud computing-based microgrids.

**INDEX TERMS** Co-simulation, GNS3, hierarchical control, MATLAB, model-based predictive control.

## NOMENCLATURE

### INDEX AND SETS

|               |                               |
|---------------|-------------------------------|
| $(\cdot)^*$   | Nominal value                 |
| $(\cdot)^p$   | Predicted value               |
| $\alpha\beta$ | Loops in $\alpha\beta$ frames |
| $\Delta$      | Input error                   |

The associate editor coordinating the review of this manuscript and approving it for publication was Huiqing Wen<sup>ID</sup>.

|           |                                   |
|-----------|-----------------------------------|
| $abc, dq$ | Loops in $abc$ and $dq$ frames    |
| $i$       | Index of participating DERs       |
| $o$       | Index of output measured variable |
| $ref$     | Reference value                   |

## PARAMETERS

|             |  |
|-------------|--|
| $\beta$     | Weight factor for the measurements of $DG_i$ |
| $\lambda_d$ | Weight factor of derivative cost function    |
| $b(k)$      | Data transmitted by secondary control        |

|                              |  |
|------------------------------|--|
| $C_f$                        | Filter capacitance                     |
| $g_{der}, g_{inv}$           | Derivative and DG cost functions       |
| $k_{p_V}, k_{i_V}$           | Controller PI parameters for voltage   |
| $k_{p_\omega}, k_{i_\omega}$ | PI controller parameters for frequency |
| $l_i$                        | Last data received by $DG_i$           |
| $m_p$                        | Frequency droop coefficient            |
| $N$                          | Number of DG                           |
| $n_q$                        | Voltage droop coefficient              |
| $R$                          | Resistance                             |
| $Z_o$                        | Output impedance for each inverter     |
| $\Delta v_{virtual}$         | Virtual impedance                      |

**VARIABLES**

|                          |   |
|--------------------------|---|
| $\Delta v_{virtual}$     | Virtual impedance                       |
| $\delta\omega, \delta V$ | Secondary control frequency and voltage |
| $\omega_i$               | Frequency amplitude of DER $i$          |
| $a(k)$                   | Global consensus average for all DGs    |
| $a_i(k)$                 | Local consensus average at $DG_i$       |
| $DG_k$                   | Broadcasted variable for all DGs        |
| $P_i, Q_i$               | Active and reactive power               |

Other notations are defined in the text

## I. INTRODUCTION

One of the most significant challenges for modern society is the transition process from fossil fuels to renewable energy, as it is essential to mitigate the effects of climate change and the negative impact of electricity generation. Microgrids (MGs) can be utilized to integrate distributed energy resources (DERs), such as photovoltaic systems (PV) or wind turbines and to reduce emissions or improve energy efficiency [1], [2].

Microgrids employ different technologies including power electronics, distributed generators (DGs), energy storage systems, loads and communications, as described in [3] and [4]. The positive effects of using MGs include: 1) reduction of transmission and distribution losses, 2) increased availability of power supply despite failures of individual units; and 3) the possibility to include additional management or control services to solve intermittent DERs problems.

Despite these benefits, variability of renewable resources and energy losses during transmission/distribution raise new challenges associated with frequency and voltage regulation [5]. A common approach to solve this problem and to achieve the microgrid operation within given standards is to use a three level hierarchical control [6]. The primary level uses the MG frequency and voltage to control power sharing between DGs. In doing so, droop control causes the bus voltage and frequency deviation from their nominal values [7].

The main drawbacks of the droop control include: 1) active and reactive coupling errors due to the impedance differences between DGs; 2) quality degradation of the shared current caused by deviations of the voltage and frequency; 3) the presence of circulating currents; 4) potential errors in active or reactive power sharing; and 5) the lack of the global measures that consider all the constraints within the

architecture [8]. Another critical issue with the traditional droop control is the slow dynamic response. To improve the system's dynamic response, alternatives to droop control have been proposed in the recent research, including Finite Control Set Model-based Predictive Control (FCS-MPC) [9], [10].

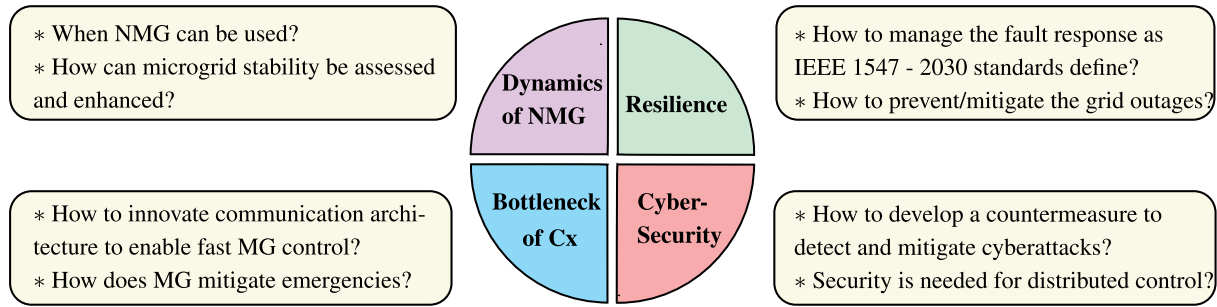
To regulate voltage and frequency deviations generated by virtual inertia and virtual impedance in the primary controllers, secondary control (SC) is typically employed [11]. Secondary control includes a communication system to regulate active/reactive power sharing and coordinate the nominal values used by DERs at the primary level [12], [13], [14]. Additionally, communications between local controllers may be used to achieve a global consensus of DERs and increase the resilience of the MG.

The communication infrastructure must provide reliable, low-latency data transmission and react quickly to dynamic network conditions (such as link failures or congestion). Fig. 1 illustrates critical challenges in networked microgrids. As follows from Fig 1, the design of scalable and resilient communications (Cx) and control infrastructure continues to be a challenge [15], [16], [17]. Furthermore, it is essential to establish an architecture that allows reconfiguration without significant modifications to the communications or control layers. Additionally, changes in the control system should not affect the communication strategy in the networked microgrid (NMG).

To prevent cascading failures and security issues in microgrids a platform capable of simulating power systems and the associated communications is essential. The use of such a platform would allow the error detection and increase interoperability of the power system. Analysis of power sharing and networked microgrid reconfiguration based on using co-simulation tools received recent attention in the published literature [6], [15], [31]. However, the existing power simulators lack the necessary detail to realistically emulate communication protocols, security issues and power devices [35], [36]. These drawbacks arise from the lack of synchronization between different subsystems. Namely, the power system simulation tools is usually proposed at fixed steps, while the communications are event-driven and take place at random time points. Also, the latency introduced by co-simulation tools affects efficiency and accuracy.

Additionally, it is very difficult to physically integrate an electrical system with communications, especially for large-scale network infrastructures. For these reasons, investigations are typically limited to studying each domain separately, without utilizing the full capacity of a global analysis.

Transmission of large amounts of data required by networked control must be secure, robust, reliable and scalable [33]. Routing protocols such as Routing Information Protocol (RIP), Open Shortest Path First (OSPF), Enhanced Interior Gateway Routing Protocol (EIGRP), and Border Gateway Protocol (BGP), limit the topology scalability and make failure detection and recovery a complex task [30]. The emergence of software-defined networks (SDN) provides an opportunity to add intelligence to the communication

**FIGURE 1.** Networked microgrid challenges.**TABLE 1.** Smart Grid/Microgrid co-simulation testbed.

| Co-simulation           | Use case   | Key contribution  | Protocols                                   | Software   |
|-------------------------|--|---|---|--|
| 2014: [18]              | Overview of available simulation techniques                              | Decision tree to select the platform  | TCP/IP (Point to Point)                     | MATLAB, OPNET, VPNET                                   |
| 2015: [19]              | Overall operation and synchronization                                    | Scheduler based on events for power and communication   | TCP/UDP (Machine to Machine (M2M))          | Adevs, MATLAB, OMNet++                                 |
| 2015: [20]              | Cybersecurity  | Security model for hierarchical control   | TCP/IP/UDP, Ethernet                        | OMNet++, IEDs with the real-time operating systems     |
| 2016: [21]              | Optimization of smart distribution networks                              | Electric Vehicle (EV) penetration, quasi real-time Volt-VAR Optimization (VVO)  | DNP.3, Ethernet                             | Real time Digital Simulator (RTDS), MATLAB             |
| 2016: [22]              | System performance   | IEC61850 Manufacturing Message Specification (MMS)  | IEC 61850 GOOSE, DNP.3, Ethernet            | MATLAB/Simulink, RTDS                                  |
| 2016: [23]              | Cybersecurity and resilience   | Impact study of common attacks in Microgrids  | TCP/IP, OPC (Open Platform Communication)   | RTDS, CORE, FreeOPCUA                                  |
| 2017: [24]              | Reliability, energy efficiency, and flexibility                          | Model Based Design (MBD) methodology, Microgrid optimization  | TCP/IP, HTTP, SCADA                         | MATLAB/Simulink, GridLAB-D,                            |
| 2017: [25]              | System performance   | IoT-aided algorithms, Turing approach and cost reduction  | TCP/UDP, IEEE 8500                          | Gridlab-D, CORE  |
| 2019: [26]              | Distributed system performance   | Impact study on dynamic phasor  | TCP/UDP, Real-time Control Protocol (RTCP)  | Real-time Digital Simulators (RTDS), VILLASnode, RSCAD |
| 2019: [27]              | Protection schemes, cybersecurity  | Multiagent system, data distribution service (DDS)  | IEC 61850                                   | GridLAB-D, NS-3, Python, HELICS                        |
| 2020: [28]              | Energy dispatch and hierarchical control                                 | Distributed optimization technique, economic dispatch   | TCP/IP sockets                              | MATLAB, DigSilent                                      |
| 2021: [29]              | Reactive power sharing, non-iterative power flow                         | Modifications of Decoupled Linearized Power Flow  | Python socket                               | PowerFactory - Python, MatrikonOPC                     |
| 2021: [30]              | Testing and validating multiple operation issues of microgrid            | Scalability of networked microgrid  | API sockets                                 | PowerFactory - Python, MATLAB, GenPred                 |
| 2021: [6]               | Reactive power control, dynamic power sharing                            | Multi-agent systems, dynamic scheduling of the battery bank   | Application socket                          | PSCAD, PADE platform                                   |
| 2021: [31]              | Interdependence between power and communications                         | Hierarchical control for large scale infrastructure, resiliency   | HELICS API                                  | GridLAB-D, NS-3, Python, HELICS                        |
| 2021: [32]              | Cooperative control  | Impact study on controllers with TCP/IP   | TCP/IP                                      | RT-LAB, OPNET  |
| 2021: [33]              | Cybersecurity, cooperative control and protection                        | Distributed control and protection with local/web-based HMI   | SMV, GOOSE, Modbus, DNP3.0                  | OPAL-RT, Hypersim, RTAC, SEL-5033 software             |
| 2022: [34]              | Electricity markets  | Architecture for active prosumer engagement   | HELICS API, ZeroMQ                          | HELICS, GridLAB-D, Python scripts                      |
| <b>2022: This paper</b> | Hierarchical control, distributed systems, cyber-security and resilience | Improved architecture and reconfiguration based on SDN, model-based predictive control, power sharing and cybersecurity | TCP/UDP, IEC 61850, IEC 61727, VDE 0126-1-1 | GNS3, MATLAB/Simulink, Python scripts                  |

infrastructure, separating the physical layer from applications and control [17]. Unlike conventional routing protocols (like RIP, OSPF, and EIGRP), SDN includes a series of open switch protocols to simplify the deployment and increase the network's resilience and efficiency. For example, after a link failure, the SDN controller recalculates the most convenient route, instructing the affected switches to use this new path. The switches will only forward data in the form of packages,

which reduces reaction times of the local controllers and improves their collaborative work.

#### A. CONTRIBUTION

This paper reviews the co-simulation tools, use cases and the most promising features such as resilience and scalability, presented in the published literature. Compared with the

existing literature and overcoming the reported constraints, the essential contributions of this paper are as follows:

- The paper proposes a novel co-simulation framework for hierarchical control of networked MGs, which combines the attractive transient capabilities of the FCS-MPC with the decentralized droop methodology.
- The paper proposes a novel control strategy based on SDN communications that increases the overall intelligence level of the system.
- The paper present a model for deploying accurate and resilient communications as an alternative to the traditional hierarchical control, power sharing and cybersecurity approaches.
- Under the proposed methodology, each DG attempts to capture the broadcast packets from other DGs, updates its local record based on the average of the references and derives the local control signal accordingly. Unlike with the conventional strategies [37], communications and control layers are not separated. Rather than waiting for a series of local data, the control signal is locally updated after each sampling period, forcing the DG towards the desired operating point.
- Cooperation between different DGs, the use of SDN technology and integration of the resilient control strategy with intelligent communications, mitigate the effects of cyberattacks and isolate the compromised nodes.

The remainder of the paper is organized as follows. Section II reviews co-simulation alternatives from the published literature, their contributions and use cases. Section III describes the architecture of the proposed co-simulation framework. Section IV presents the proposed communication algorithm. Sections V and VI detail the primary control methodology under droop control and FCS-MPC, respectively. Section VII describes the adopted secondary control strategy. The results and discussion are presented in Section VIII. The security issues and mitigation strategy are presented in Section IX. Section X concludes this paper and outlines the future research directions.

## II. LITERATURE REVIEW

Various power simulation tools are available to evaluate the performance of control algorithms, power exchange methods, fault reduction strategies and to study economic power dispatch. The most common simulators are MATLAB/Simulink, OpenDSS, PowerWorld, PSLF (Positive Sequence Load Flow), PSS/E and Modelica. To evaluate new communications architectures and protocols in power systems, network simulators such as NS2, NS3, OMNet++, NeSSI and OPNET Modeler have been used [15]. Table 1 shows the most recent developments on co-simulation platforms for smart grids and microgrids.

Only a limited number of papers [20], [23], [27], [33] include elements of security in a simulation environment. The emergence of new security threats and the economic impact on the utility system shifts the research attention to

alternatives that improve network performance and reduce microgrid vulnerabilities [38], [39], [40]. It is then imperative to evaluate the effects of these types of threats and the ability of the microgrid to cope with these security breaches.

An alternative approach is to use testing platform based on hardware in the loop (HIL), as a tool for real-time microgrid emulation. The testing platforms, such as OPAL-RT or dSPACE, are known for their high cost. They have limitations with respect to analyzing security issues, for which they require additional software licenses [41]. The above limitations reduce their value for relatively small research centers. This further highlights the importance of a global framework to enable power-sharing, communications architecture design and security evaluation, at a reduced cost.

In [37], a distributed averaging proportional-integral (DAPI) control strategy is proposed for frequency and voltage regulation in a hierarchical microgrid. This strategy implements power exchange using low communication bandwidth and provides the infrastructure's plug-and-play capability. However, the system has high latency and cannot compensate for packet loss due to failure of one of the communication devices.

Model-based Predictive Control (MPC) is a possible solution to the problem of packet loss and high latency. In [42] and [43] a distributed predictive control scheme (DMPC) is proposed that includes the latency and packet loss constraints within the optimization problem. Although very promising, this proposal assumes that the communication protocol is ideal and leaves out of the scope other types of failures, such as those caused by path loss or cyberattacks. In addition, variability of the network topology needs to be further addressed at the secondary control level. Therefore, a strategy that adds resilience, intelligence and scalability to the communication infrastructure remains as open issue.

## III. CO-SIMULATION ARCHITECTURE

Considering previous research [6], [17], [36], [37], the study presented in this paper is based on the use of the hierarchical control strategy, which increases the microgrid's resilience and reconfiguration capacity. The proposed architecture is shown in Fig. 2. This architecture utilizes MATLAB/Simulink to implement the electrical system and GNS3 as a networking simulation tool.

The electrical system and model-based predictive control are developed in MATLAB/Simulink (step ① of Fig. 2), which is well-suited to the requirements of control strategies and power electronics devices. The example presented in this work includes four Voltage Source inverters (VSI), interconnected through line impedances. Each inverter is controlled by FCS-MPC, which improves dynamic response [44] and adds the capacity to send/receive information in real-time from/to GNS3 (steps ② and ③ of Fig. 2).

GNS3 [45] is an open-source network simulation tool that emulates a complex communication network through a graphical user interface. It is based on Dynamips / Dynagen emulator [46]. The most important features of GNS3 are the

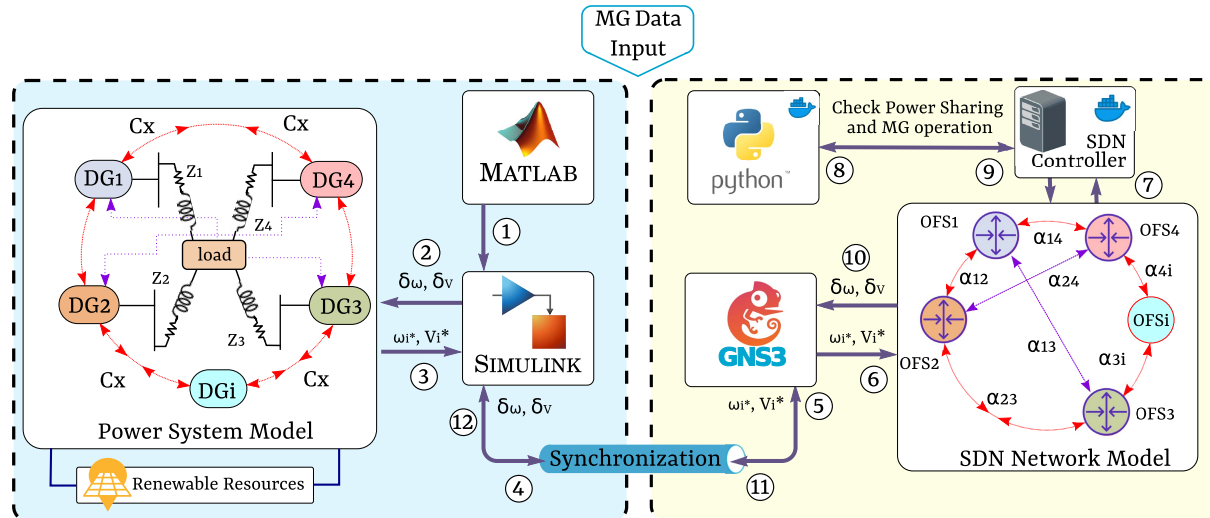


**FIGURE 2.** Proposed architecture for co-simulation framework. Dashed lines between DGs represent communication links.

ability to run Docker containers inside the communication architecture and to include virtual machines in the runtime environment. These features allow complex communication devices such as open-flow switches, SDN controllers, or conventional routers, to be included within the topology without the need for additional resources. Also, this tool enables packet capture in real-time, analyzes the traffic, allows to introduce jitter and packet losses, and to simulate different disturbances, such as link/device failures or congestion.

Another SDN simulation alternative is Mininet [47], which has become increasingly popular in recent years. However, it is mainly focused on SDN networks, which decreases the versatility of the communication architecture under study. The topology implementation in Mininet is relatively complex and requires Linux. Another prominent disadvantage of Mininet is that it cannot natively run Docker containers or virtual machines. The above limitations of Mininet, plus the lack of scalability options, especially those required by cybersecurity, makes GNS3 a preferred candidate.

The GNS3 topology comprises four OpenFlow Switches (OFS), supervised by an OpenDaylight SDN controller, implemented in a Docker container [48]. The advantages of using the Docker are in reducing the deployment time and packaging of the applications. Secondary controllers are deployed at each Docker container. Furthermore, a Python application running inside another container coordinates MATLAB dynamic simulations and data exchange through the SDN network in GNS3. This Python application aims to calculate the voltage and frequency references for the global power sharing and reconfiguration signals for the inverters. The block on the right hand side of Fig. 2 shows the communication architecture. The MATLAB and GNS3 parts are interconnected by a synchronization mechanism.

Synchronization is performed through User Datagram Protocol (UDP) socket at each sampling period of MATLAB

(steps ④ and ⑪ of Fig. 2). It is preferred to use UDP instead of Transmission Control Protocol (TCP), to take advantage of the connection-less protocols, referring to high speed and lower transmission rate in case of errors. In this way, if a failure occurs when receiving a message, the references will be set to the previous values until the next sampling period. The sampling error is minimized by using a default buffer connected to UDP Block at each local controller, according to the logic proposed in [49].

The reference and reconfiguration values are sent over the SDN network, which is controlled by OpenDaylight [50] in GNS3 (steps ⑥ and ⑦ of Fig. 2). The Python application (steps ⑧) recalculates the voltage reference for power-sharing and sends the result back to MATLAB/Simulink (steps ⑨ and ⑩ of Fig. 2). Upon receiving the new settings, Simulink reconfigures the microgrid, forcing it to modify the current conditions if necessary (steps ⑪ and ⑫ of Fig. 2).

The OSPF communication protocol is compared with SDN to evaluate the performance of the microgrid communication strategy. The goal is to estimate the routing convergence time for both protocols without bandwidth limitations or link delays. The communication starts in Simulink and is established between DG1 and DG4 by firing a continuous message over the main path. The route is detected using the *traceroute* command. A link and device failure is simulated for 10 seconds and then the simulation waits until reconnection via an alternate route is achieved. The next step is to determine the convergence time and the number of packet losses. As shown in Fig. 3, SDN has lower convergence time and significantly fewer packet losses during failure and reconnection than OSPF.

To test critical scenarios, Fig. 4 compares typical responses of OSPF and SDN to a failure. The plot on the right hand side illustrates the worst case scenario with a 10 ms delay and 10 ms jitter. As can be seen, even near the maximum

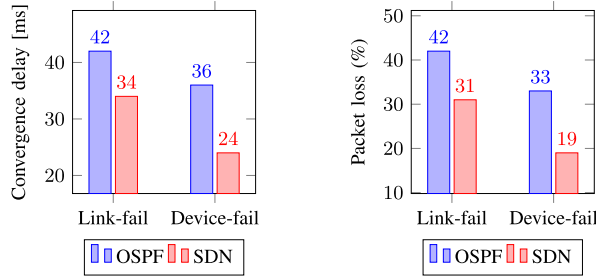


**FIGURE 3.** Routing convergence delay and packet loss when link failure and device failure for OSPF and SDN.

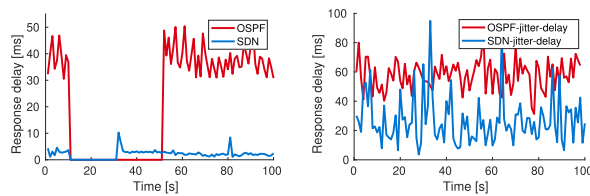


**FIGURE 4.** Measured latency during OSPF and SDN communication. At 10 seconds on the left side, communication device failure occurred. The performance for 10 ms delay and 10 ms jitter is on the right side.

value of jitter allowed in communications networks [51], the framework's performance remains stable.

The main drawback of using GNS3 is its high demand for computational resources. According to [52], computational requirements of Mininet and GNS3 are similar, especially when they run in Linux environments. The co-simulation results in this work are obtained in Linux environment with an i5 processor and 32 GB of RAM.

#### IV. PROPOSED COMMUNICATION ALGORITHM

The communication strategy is based on a gossip broadcast algorithm for achieving consensus [53]. Gossip algorithms have received the research attention due to their ability to compute global statistics (like average methods) using local pair-wise communications [54].

Here, for simplicity, it is assumed that all DGs are connected. The distributed averaging algorithm uses a global variable  $\delta x$ , representing a secondary control objective (for example, voltage or frequency). At each sampling time  $k$ , the measurements  $\delta x_i(k)$  are made, and the global average  $a(k)$  is calculated by the Python application for the  $DG_i$ . The signal transmitted at each sample  $k$  can be calculated as described in [55], where  $N$  means the DG number:

$$b(k) = a_i(k), i = 1, 2, \dots, N \quad (1)$$

The local estimate values  $a_i(k)$  of all DGs, including the broadcasting one, are updated as follows [56]:

$$a_i(k) = \beta \delta x_i(k) + (1 - \beta_i) b_i(k), \quad i = 0, 1, \dots, N - 1 \quad (2)$$

where  $b_i(k)$  is the local record of the received broadcast data:

$$b_i(k) = b(l_i), \quad l_i < k \quad (3)$$

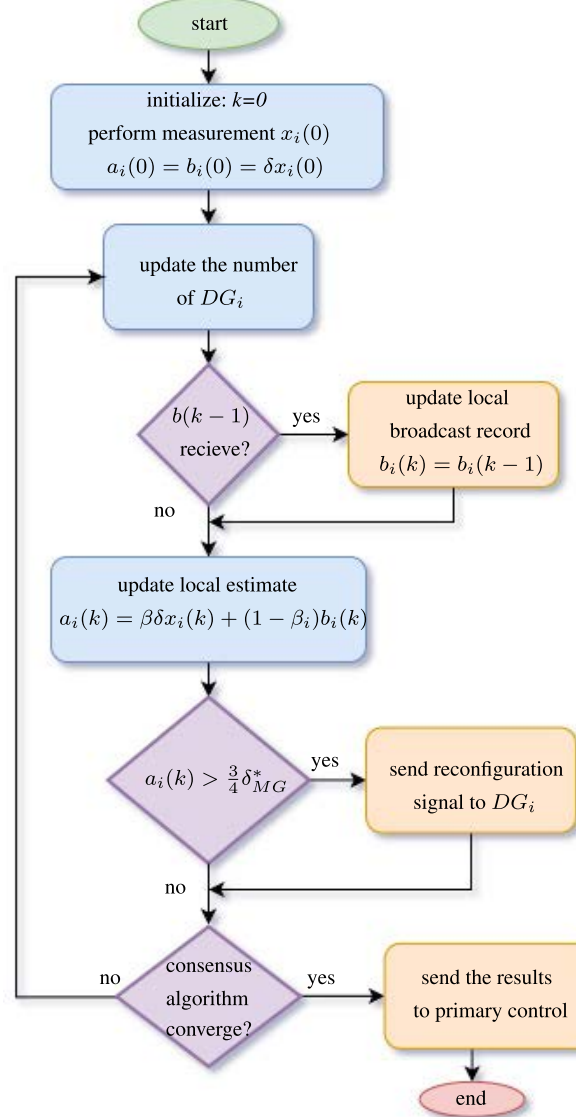


**FIGURE 5.** Implemented gossip broadcast algorithm. Modified from [55].

Variable  $l_i$  represents the last data correctly received by the  $DG_i$ . If the communication takes place in an environment without packet losses then  $b_i(k) = b_i(k-1)$ ,  $i = 0, 1, \dots, N - 1$ . The value  $\beta$  is included as a weighting factor to limit the gain measurements made by  $DG_i$ . Choosing  $\beta_i = 1/N$ ,  $i = 0, 1, \dots, N - 1$ , simplifies the communication strategy. Fig. 5 shows the communication flowchart for one DG.

In a typical co-simulation networked MG, the propagation latency can be neglected, and the dominant contributor to the delay is the protocol stack processing [17]. For these reasons, the delay is only considered during the reception, average estimation and the data broadcasting. Next, the voltage and frequency reference, generated by the communications strategy, is passed to the primary control. The primary and secondary control algorithms have been developed, to evaluate

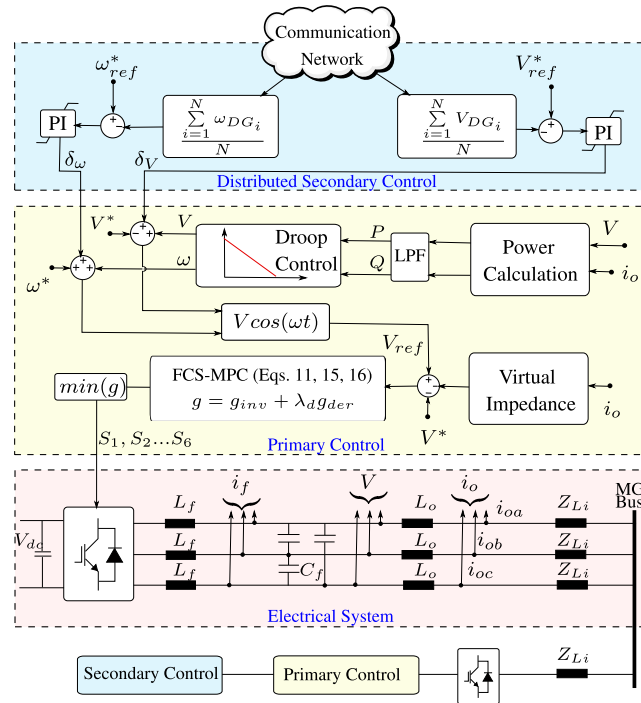


**FIGURE 6.** Proposed topology of the secondary distributed control strategy.

the overall performance of distributed microgrid control and the impacts of communications, as described below.

## V. BUILDING DROOP WITHIN PRIMARY CONTROL

The adopted microgrid topology includes parallel inverters and multiple loads connected to the common AC bus (see the Electrical System shown in Fig. 6). The droop control strategy is used to regulate the MG power sharing. The main goal of the primary droop control is to set an equitable load sharing amongst the DGs, based on a well known P-Q droop method [37]. Each inverter has an external droop control loop, to establish decentralized control. The Primary Control block shown in Fig. 6 details the adopted strategy used in this work to regulate frequency and voltage.

Using the droop principles, the frequency and voltage amplitude of each inverter is given by, respectively:

$$\omega_i = \omega^* - m_p(P - P^*) = \omega^* - m_p \Delta P \quad (4)$$

$$V_i = V^* - n_q(Q - Q^*) = V^* - n_q \Delta Q \quad (5)$$

where  $\omega^*$  and  $V^*$  are the nominal frequency and voltage,  $P$  and  $Q$  are the measured active and reactive power injections and  $\Delta P$  and  $\Delta Q$  are the corresponding power inputs errors for the droop controller. Coefficients  $m_p$  and  $n_q$  regulate maximum deviations allowed within the MG [36].

Different lengths of transmission lines make the output impedances of the the voltage source inverters unequal, causing unbalanced power sharing under droop control. The virtual impedance concept is then used to achieve a fixed output impedance value and to decouple the control of active and

reactive powers [9]. The virtual impedance helps to keep the voltage within the defined limits. Additionally, it provides harmonics compensation and improves the system stability.

### A. VIRTUAL IMPEDANCE

The idea of virtual impedance is to emulate the behavior of a real impedance without introducing the associated losses. Fig. 6 shows the input and output signals in the Virtual Impedance block. In this work, the Virtual Impedance block is implemented based on the ideas presented in [36], considering the distribution lines as inductive:

$$V_{ref} = V^* - Z_v \cdot i_o \quad (6)$$

where  $Z_v$  is the inductive virtual impedance,  $V^*$  is the nominal voltage measured across the LCL filter capacitor, and  $V_{ref}$  is the voltage reference provided by the outer droop control. The LCL filter is designed according to [57] and is intended to keep the voltage drop caused by the virtual impedance within the desired limits.

The virtual impedance values is then selected such as to achieve equal equivalent output impedances across all the inverters. A positive impedance  $Z_v$  is added to the inverter with a lower physical output impedance and adds a negative virtual impedance to the inverter with a higher physical output impedance.

Equation (7) shows how virtual impedances are added for the two adjacent DGs. In each case, two virtual impedances are added. The combination of the two virtual impedances results in the same power-sharing performance as with the conventional single virtual impedance, but the voltage drops across the virtual impedances are significantly reduced [57]:

$$Z_{o,1} + Z_{v,1} = Z_{o,2} + Z_{v,2} \quad (7)$$

where  $Z_{o,i}$  denotes the output impedance of inverter  $i$  and is the sum of all impedances between the inverter's output and the load; and  $Z_{v,i}$  is half the value required to equalize the output impedances.

Virtual impedance loops ( $\Delta v_{virtual,abc}$ ) are impelmented in a synchronous reference frame using per unit values. This provides compatibility of the different control levels with each other:

$$\Delta v_{virtual,abc} = RL \frac{di_{abc}}{dt} \quad (8)$$

Applying Park transformations, equations (9) and (10) for the synchronous reference frame can be obtained as:

$$\Delta v_{virtual,dq} = R_{i,dq} L \frac{di_{dq}}{dt} + j\omega L i_{dq} \quad (9)$$

$$\begin{bmatrix} \Delta v_{virtual,d} \\ \Delta v_{virtual,q} \end{bmatrix} = R \begin{bmatrix} i_d \\ i_q \end{bmatrix} + L \cdot s \begin{bmatrix} i_d \\ i_q \end{bmatrix} + \begin{bmatrix} 0 & -\omega L \\ \omega L & 0 \end{bmatrix} \begin{bmatrix} i_d \\ i_q \end{bmatrix} \quad (10)$$

In the published literature, droop control is widely used for both the inner and the outer control loops. However, this approach suffers from severe practical limitations due to the fact that the outer loop needs to be designed with a smaller

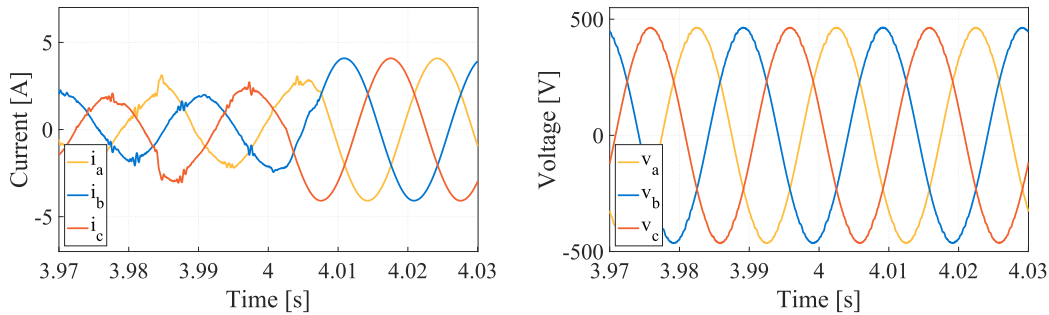


**FIGURE 7.** Current  $i_{abc}$  and voltage  $V_{abc}$  regulation, when DG 1 is disconnected at 4s.

bandwidth than the inner control loop [9]. Additionally, active and reactive coupling errors and the potential phase shifts under such a control may result in slow transient response.

These problems can be addressed by using Finite Control Set Model Predictive Control (FCS-MPC), as discussed in the next section.

## VI. PRIMARY CONTROL BASED ON FCS-MPC

FCS-MPC is based on a discrete-time model used to predict the future behaviour of a controlled variable. In each cycle, it implements a single optimal switching state, without the use of modulation [9]. The optimal state is selected, from a finite control set, so as to minimize a given cost function.

As is common in the literature [44], it is assumed that each DG interfaces with the MG loads via a Voltage Source Inverter (VSI). A cost function considering the currents in coordinates  $\alpha$ ,  $\beta$ , is obtained through equation (11). For simplicity, it is assumed that the reference voltage does not significantly change over a sampling interval, so  $V^*(k+1) = V^*(k)$ . This assumption can introduce a sample delay, which is not a problem when using high sampling frequencies. A quadratic cost function is then defined as follows:

$$g_{inv} = (V_\alpha^* - V_\alpha^p)^2 + (V_\beta^* - V_\beta^p)^2 \quad (11)$$

where voltages  $V_\alpha$  and  $V_\beta$  are calculated based on Clark transformation for nominal (\*) and predicted values ( $p$ ).

The reference voltage as function of time is given by:

$$V^*(t) = \underbrace{V_{ref} \sin(\omega_{ref} t)}_{V_\alpha^*(t)} + j \underbrace{V_{ref} \cos(\omega_{ref} t)}_{V_\beta^*(t)} \quad (12)$$

where  $V_{ref}$  and  $\omega_{ref}$  are the voltage amplitude and the angular frequency ( $\omega_{ref} = 2\pi f_{ref}$ ) of the reference signal at time  $t$ . The derivative of the voltage reference can be obtained as:

$$\frac{dV^*(t)}{dt} = \underbrace{\omega_{ref} V_{ref} \cos(\omega_{ref} t)}_{\omega_{ref} V_\beta^*(t)} + j \underbrace{\omega_{ref} V_{ref} \sin(\omega_{ref} t)}_{\omega_{ref} V_\alpha^*(t)} \quad (13)$$

To track  $V^*(t)$ , equations (12) and (13) are converted to the  $\alpha$ ,  $\beta$  frame. The predicted current  $i_f$  and the measured current  $i_o$  are calculated as explained in [9], to predict the

capacitor voltage derivative as:

$$\frac{dV^*(t)}{dt} = \underbrace{\frac{i_{f\alpha}(t) - i_{o\alpha}(t)}{C_f}}_{\frac{dV_\alpha^*(t)}{dt}} + j \underbrace{\frac{i_{f\beta}(t) - i_{o\beta}(t)}{C_f}}_{\frac{dV_\beta^*(t)}{dt}} \quad (14)$$

where  $i_f(t)$  and  $i_o(t)$  are the current measured in the LCL filter, and the output current of the DG, respectively.

From equation (14) it follows that the derivative part of the voltage, can be tracked if the error between the predicted and the measured currents is minimized. Then the corresponding cost function can be formulated as:

$$g_{der} = (C_f \omega_{ref} V_\beta^* - i_{f\alpha} + i_{o\alpha})^2 + (C_f \omega_{ref} V_\alpha^* + i_{f\beta} - i_{o\beta})^2 \quad (15)$$

Building on the the above discussion, the total cost function can be defined as a sum of the conventional cost function (11) and the cost function (14) for the voltage derivative across the capacitors. The weighting factor  $\lambda_d$  in the total cost function allows for adjusting the effect of the derivative term:

$$g = g_{inv} + \lambda_d g_{der} \quad (16)$$

Fig. 7 shows the results of the model-based predictive control during a microgrid reconfiguration. It can be seen that the proposed control algorithm provides fast dynamic response, which adds to the MG's resilience. The voltage and frequency deviations caused by the droop control are eliminated by the secondary control, which is discussed next.

## VII. SECONDARY CONTROL

Secondary control allows for regulating the microgrid voltage and frequency altered by the primary control. In this paper, a local secondary controller is implemented at each DG, as opposed to using a centralized secondary control strategy [17].

### 1) FREQUENCY CONTROL

Each DG measures its own frequency at each sampling instant ( $\omega_{DG_i}$ ), averages the received information from other units ( $\omega_{DG_k}$ ) and then broadcasts its calculated average frequency ( $\delta\omega_{DG_k}$ ) to the DGs. Then, the average is compared with the

**TABLE 2.** Electrical and control parameters of the MG.

| Parameters                           | Value               | Measurement                 |
|--------------------------------------|---------------------|-----------------------------|
| Load power rating                    | 5.7                 | [kVA]                       |
| Nominal voltage                      | 400                 | [V]                         |
| Nominal frequency                    | 50                  | [Hz]                        |
| Inverters side inductor              | 500                 | [ $\mu$ H]                  |
| Inverters side resistor              | 0.28                | [ $\Omega$ ]                |
| Capacitor                            | 50                  | [ $\mu$ F]                  |
| Grid side inductor                   | 200                 | [ $\mu$ H]                  |
| Line impedance 1 and 3               | $0.1488 + j0.4969$  | [ $\Omega$ ]                |
| Line impedance 2 and 4               | $0.0930 + j0.3100$  | [ $\Omega$ ]                |
| Virtual impedance 1 and 3            | $-0.0279 - j0.0935$ | [ $\Omega$ ]                |
| Virtual impedance 2 and 4            | $0.0279 + j0.0935$  | [ $\Omega$ ]                |
| P - $\omega$ Droop Coeff. ( $m_p$ )  | $2.5937 * 10^{-4}$  | [ $\frac{rad}{W \cdot s}$ ] |
| Q - V Droop Coeff. ( $n_q$ )         | $1.5 * 10^{-3}$     | [ $\frac{Var}{V}$ ]         |
| Weighting factor FCS-MPC $\lambda_d$ | 0.2                 | -                           |
| Frequency proportional term $k_p f$  | 0.01                | -                           |
| Frequency integral term $k_i f$      | 3                   | $s^{-1}$                    |
| Voltage proportional term $k_p E$    | 0.01                | -                           |
| Voltage integral term $k_i E$        | 2                   | $s^{-1}$                    |

nominal frequency of MG ( $\omega^*$ ) and sent to the secondary  $DG_i$  controller, to restore the frequency as follows:

$$\omega_{DG_i}(t) = \omega_o + m_p P_i(t) + \delta\omega_{DG_k} \quad (17)$$

$$\omega_{DG_k} = \frac{\sum_{i=1}^N \omega_{DG_i}}{N} \quad (18)$$

$$\delta\omega_{DG_k} = k_{p_\omega}(\omega^* - \omega_{DG_k}) + k_{i_\omega} \int (\omega^* - \omega_{DG_k}) dt \quad (19)$$

where  $k_{p_\omega}$  and  $k_{i_\omega}$  are the PI controller parameters;  $\delta\omega_{DG_k}$  is the compensation signal for the primary control (see to Distributed Secondary Control block shown in Fig. 6);  $\omega_{DG_k}$  is the average frequency determined by  $DG_k$ ; and  $\omega^*$  is the nominal frequency of the MG.

## 2) VOLTAGE CONTROL

After calculating the voltage average ( $V_{MG}$ ) received from the communication network, the local controller determines the error between this value and the reference output voltage  $V^*$ . This error  $\delta V_{DG_k}$  is then sent to the primary control (FCS-MPC) to compensate for the voltage deviation. Fig. 6 shows the described strategy in the Distributed Secondary Control block.

$$V_{DG_i}(t) = \omega_o + n_q Q_i(t) + \delta V_{DG_k} \quad (20)$$

$$V_{DG_k} = \frac{\sum_{i=1}^N V_{DG_i}}{N} \quad (21)$$

$$\delta V_{DG_k} = k_{p_v}(V^* - V_{DG_k}) + k_{i_v} \int (V^* - V_{DG_k}) dt \quad (22)$$

where  $V_{DG_k}$  is the average of voltages broadcasted from all DGs. Small signal representations of frequency and voltage for secondary control are detailed [36].

## VIII. RESULTS AND DISCUSSION

Performance of the proposed framework, control strategy, and the intelligent communication system was validated on a modified IEEE 5 bus system [11]. To perform the evaluation, a MATLAB simulation was implemented using the parameters detailed in Table 2. Different test cases were considered including droop control, virtual impedance, secondary

control and communications cybersecurity analysis. In each case, voltage and frequency comparisons were performed. Each simulation length is 10 seconds. The distributed control strategy uses SDN as an alternative to the conventional communication strategy and the associated protocols.

As is common for a small scale microgrid, the distribution lines are assumed to have inductive behavior [57]. The lengths of these lines are 500 meters for inverters one and three ( $Z_1, Z_3$ ) and 800 meters for inverters two and four ( $Z_2, Z_4$ ). The microgrid includes two linear loads, and four identical VSIs with equal shares. The loads are resistive-inductive, which enables studying the active and reactive power sharing. The loads are modeled as constant impedance and their size is chosen to represent the residential loads.

### CASE 1 (DROOP CONTROL WITHOUT COMMUNICATION)

During the time between 0 and 1 second, only droop control with virtual impedance is implemented, with no communication links between the DGs. Figs. 8, 9 show the simulation results. The output voltage and current are regulated around the nominal values. However, power sharing, frequency and voltage amplitude (Fig. 9) deviate from the nominal values. Depending on the initial conditions and controller gains, frequencies  $\omega_i$  may converge to different values and shift their respective droop curves by different amounts. This unwanted degree of freedom causes unequal active power sharing, as seen in Fig. 8 between 0 to 1 second.

### CASE 2 (ADDING SECONDARY CONTROL)

At the time 1s and up to the end of the simulation, the communication links and average estimation algorithm are added. The averaging algorithm minimizes the frequency error at the primary control level and provides equal power sharing between DGs. As shown in Fig. 9, the proposed strategy restores frequency and voltage faster than the strategy with only primary control.

### CASE 3 (CHANGING THE AC LOAD)

Starting at 2 seconds and until 5 seconds, an additional 25% load is added to the MG bus. This leads to an increased active power supplied by the inverters. Furthermore, between 5 and 10 seconds, the load-shedding of the biggest impedance is simulated. Figs. 8, 9, show the results.

### CASE 4 (ADDING OR REMOVING DGs)

At the time 8s and up to the end of the simulation, the Python script in GNS3 sends a disconnection signal for DG1. As can be seen in Figs. 8, 9, the removal of the DG1 from the MG is successful and the SDN communication strategy performs as expected.

Plug and play capability in a microgrid is essential to ensure its resilience. To illustrate this, the Fig. 10 shows a comparison between the primary control and the proposed strategy under simulated disconnection and reconnection of a DG. In this case, at time 2 seconds the DG1 is disconnected and then reconnected again at 4 seconds. During the

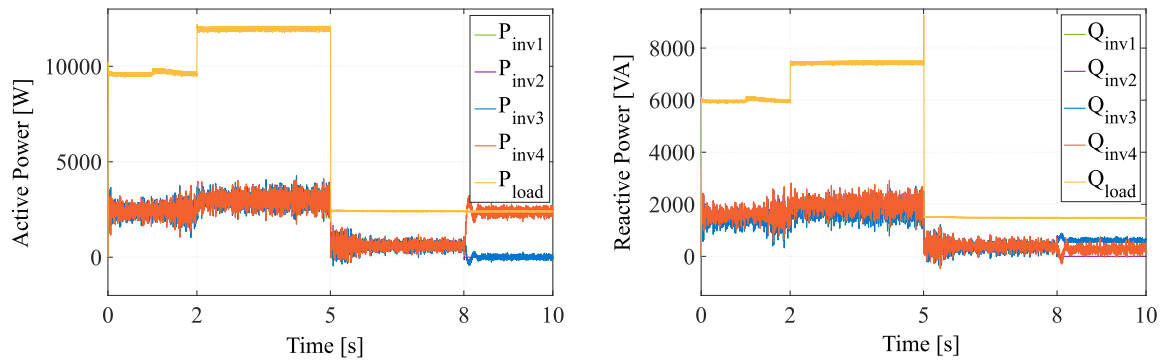


**FIGURE 8.** Performance of active and reactive power sharing strategy.

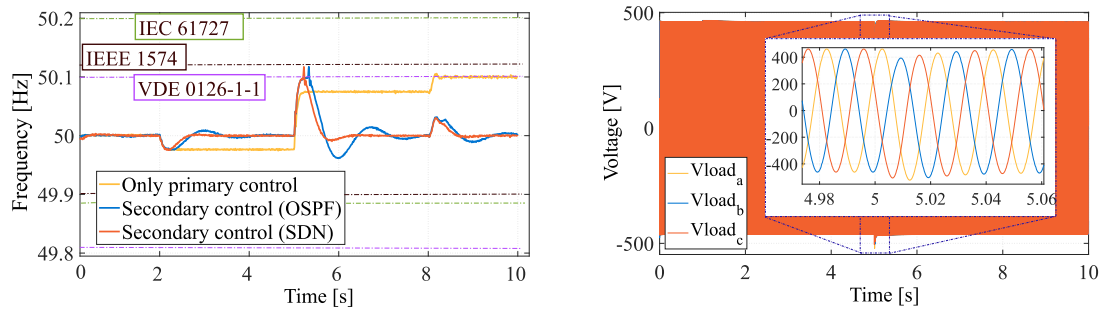


**FIGURE 9.** Comparison of frequency and voltage restoration for primary control, OSPF and proposed distributed secondary control.

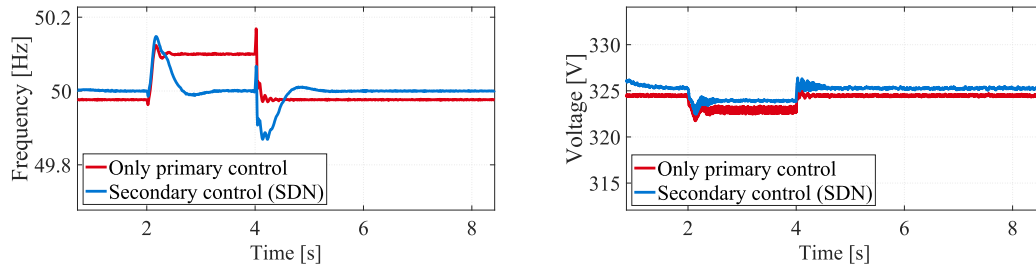


**FIGURE 10.** Performance distributed strategy with DG switching off/on. For  $0 < t < 2$ s, all DGs are connected. At  $2 < t < 4$ , the DG<sub>1</sub> is disconnected, simulating a failure. When  $4 < t < end$ , DG<sub>1</sub> is reconnected to the microgrid.

reconnection, deviations of voltage and frequency are produced, which are then eliminated approximately 1 second later. This behaviour is acceptable according to [58]. Also, as shown in Fig. 10, the proposed strategy performs much better than the primary control alone. The frequency deviations are within the limits defined by the standards IEEE 1574 and IEC 61727 [36].

It is worth noting that the response time of the secondary control can be reduced by increasing the gains of PI controllers. However, the achievable bandwidth is limited by the communication network and the bandwidth of the primary control. The current and voltage calculated by FCS-MPC during the step changes validate the performance of the primary control. As can be seen in Figs. 7 and Fig. 10, the current and

voltage of the MG Bus are appropriately regulated during the disconnection of the DG1 at 4 seconds.

According to the presented simulation results, in all cases it is possible to regulate the voltage and frequency towards their nominal values. In the first part of the simulation ( $0 < t < 1$ s), with only droop control and virtual impedance, reaching steady state for frequency has some limitations. When secondary control kicks in ( $1 < t < end$ ), a more accurate frequency regulation is achieved. The proposed secondary control algorithm allows for regulation of both frequency and voltage, despite rapid changes in the load. Therefore, the combination of the Python application in GNS3, consensus algorithm and FCS-MPC results in a reconfigurable microgrid resilient against disturbances in the load

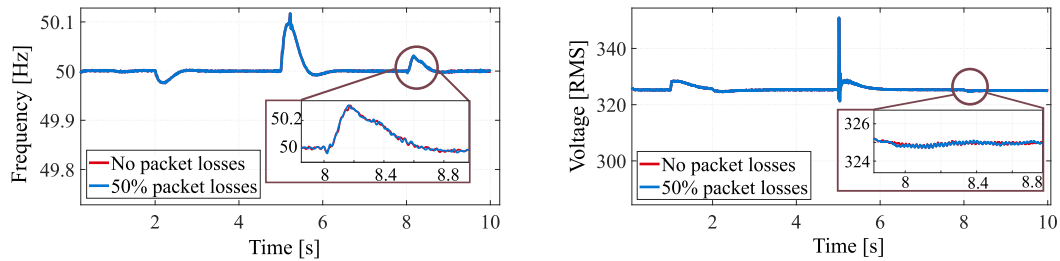


**FIGURE 11.** Frequency and voltage restoration for 50% of the packet losses and 100 ms delay. For  $0 < t < 1$ s, only primary control are considered, at  $1 < t < end$ , the secondary control is activated. When  $2 < t < 5$ s, load is added and  $5 < t < end$  higher load is disconnected. Finally at 8s, DG<sub>1</sub> is turned off.

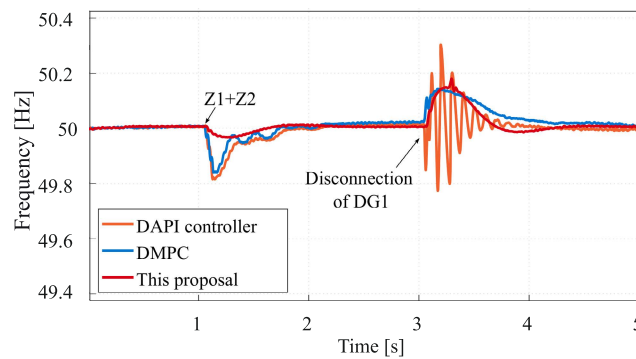


**FIGURE 12.** Comparison of microgrid frequency response for Distributed Average PI control (DAPI), Distributed Model-based Predictive Control (DMPC) and this proposal.

or distributed generators. As can be seen in Fig. 9 the SDN-based strategy performs better than its competitors and achieves a steady state faster.

#### A. COMMUNICATIONS LINK FAILURES

The impact of packet loss due to poor communication system performance is further evaluated. Fig. 11 shows results for a 50% of packet loss and a 100 ms communication delay. When this happens, a high frequency deviation is initially observed. After less than a second the frequency is stabilized to its nominal value. A memory block is introduced within the secondary control to minimize the effect of packet loss [49]. This allows the system to feed the PI controllers with the last value received by the gossip algorithm if the communication system fails.

#### IX. STABILITY

Stability analysis in networked microgrids is vital to guarantee the electrical system's reliability in the face of DERs variability or load changes. In [59], a comparative analysis under different disturbances of a networked microgrid is performed. Similarly, in [36], it is shown that when using load frequency analysis and safe switching sequence the frequency/voltage deviations are eliminated faster than with the traditional linear control approach. To limit the switching effort and to decrease the total harmonic distortion (THD) the corresponding terms can be added to the primary control cost function. A detailed

analysis of stability and harmonic distortion can be found in [60] and is out of scope of the current paper.

Here, to illustrate stability, the frequency control results for the proposed strategy is compared with two well-cited distributed control strategies [37], [42]. Under this scenario, an additional load is connected to the power system at  $t = 1$ . After 2 seconds, the simulation disconnects one of the DGs involved in the microgrid power exchange. As can be seen in Fig. 12, the dynamic performance of the proposed control is superior to both DAPI [37] and DMPC. The effort of the DMPC predictive control strategies and this proposal is similar and less than that required by the DAPI control, which looks near to the unstable conditions. However, the steady state is reached in approximately 1 second in all cases.

The use of the proposed strategy is particularly advantageous in the situation of load increase or disconnection. This is due to the high bandwidth, and the use of intelligent communications system. In this sense, to improve the performance of optimal frequency control, the researches [61], [62] propose the application of imperialist competitive algorithm (ICA) and dual-stage fractional order PID to enhance frequency control in an NMG. From the comparative point of view, both strategies minimize the frequency deviation through classical PI control modifications. These parameters include ICA, to minimize a cost function and improve the system's dynamic response to disturbances. An exciting alternative to adding more intelligence to the above control systems is presented in [63], where fuzzification and filtering strategies are applied to optimize coefficients and improve frequency control.

FCS-MPC improves the dynamic response of the primary control. As discussed in the literature [36], [64], FCS-MPC demonstrates faster frequency and voltage regulation than the conventional PI primary control. Also, the VSC switching harmonics can be effectively suppressed.

Stability under cyberattacks presents challenges that have not been sufficiently addressed in the literature [65]. For example, synchronization of multiple DERs [66], as well as minimization of stability times, especially during transitions/failures [67], still require further work. Some researchers [68], [69], [70], have demonstrated asymptotical stability of their control architectures using Lyapunov's theory [71]. Also, in [36], a stability analysis of the primary

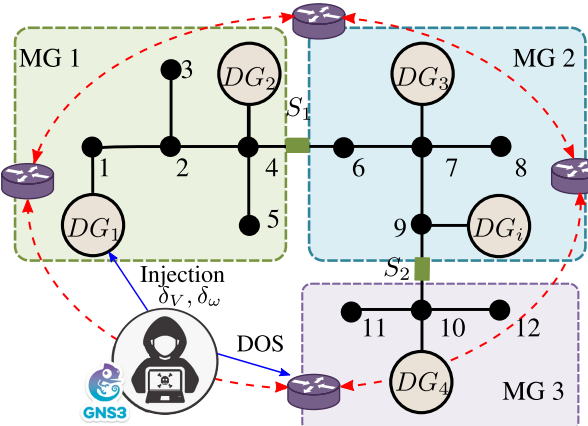


**FIGURE 13.** Injection and DOS attacks in IEEE 5 Bus testbed architecture.

frequency and voltage control is performed by using the describing functions.

Attacks aimed at inducing errors in the frequency control seek to degrade the stability of the electrical system through the injection of control errors. Some recent suggestions to mitigate these threats consider using energy storage systems to ensure transient stability [72].

## X. SECURITY ANALYSIS OVER NMG

Cybersecurity is one of the most critical challenges of today's networked microgrid [38]. The data availability, integrity and reliability are essential in avoiding negative economic and physical impacts. In addition to improving reliability, increasing resilience and adding intelligence to the communications system, SDN can also detect cyber-attacks and improve the security. In [73] a model to mitigate power bot attacks through a series of detection rules on the SDN controller is presented. However, it is only focused on hijacking attacks, leaving out other common scenarios. In [74], a programmable SDN controller is presented to detect complex cyber-attacks. In [75] a resilient control against false data injection in NM is discussed, that is based on Weighted Mean Subsequence Reduced (W-MSR).

However, the above strategies cannot integrate SDN, to distinguish between different threats. The minimum bandwidth utilization, denial of service attacks (DoS), false data injection techniques (FDI) and controller hijacking are the most important risks in NM [68], [76]. False data injection (FDI) and hijacking attacks can affect the inverter's data integrity (and modify control strategy), while DoS attacks harm the availability of the communications service.

This paper proposes a new intelligent strategy to detect and mitigate DoS and FDI attacks embedded in the proposed framework. Fig. 13 shows a scenario, in which a virtual machine in GNS3 with ParrotOS performs a DoS attack and FDI attack. To illustrate the worst case scenario, the DoS attack is carried out on the communication device that connects the SDN with MATLAB. The DoS attack targets the

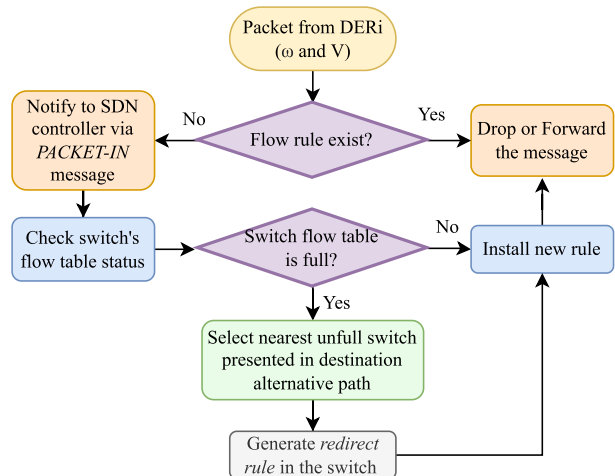


**FIGURE 14.** Flow chart of the strategy against cyber attacks in the proposed SDN framework.

communications device closest to  $DG_4$ , while the FDI attack aims at the DSP controller within  $DG_1$ .

The algorithm applied in this case is shown in Fig. 14, where a series of small control signals and decision rules are implemented in the SDN controller. The proposed approach increases resilience of NM with minimal intervention of the SDN controller and bandwidth utilization and allows for the deployment of different cybersecurity test scenarios.

As Figs 15, 16, 17, 18 show, the distributed control strategy without considering cyber attacks is highly vulnerable to FDI and DoS attacks. The control variables such as frequency and voltage under attack become unstable, causing the MG to collapse. The simulations evaluate the power exchange under FDI and DoS attacks and demonstrate that it is essential to include the cyber attack mitigation within the microgrid control strategy. In the literature various intrusion detection systems are proposed, to alert or prevent cyberattacks [77]. However, when operating under a distributed control strategy, nodes are only able to identify threats locally, without a global perspective of collaborative work.

Another technology offering clear benefit to smart grid and microgrid security applications is blockchain technology. Unlike intrusion detection systems, it involves a peer-to-peer communication based on a cryptographic transaction [78], [79]. This alternative is ideal for distributed system applications, such as electrical systems. In addition, to improving reliability and security, the blockchain technology can provide data integrity.

## A. MITIGATION OF INTEGRITY-ORIENTED ATTACKS

The most critical risks for the data integrity in the inverter control applications are FDI and hijacking attacks. Based on the procedure presented in [73], it is proposed here to use a host tracking service (HTS) to prevent corruption of the inverter control parameters by an attacker. The HTS service uses the *HostStatus\_Checker* flag on the incoming packets,

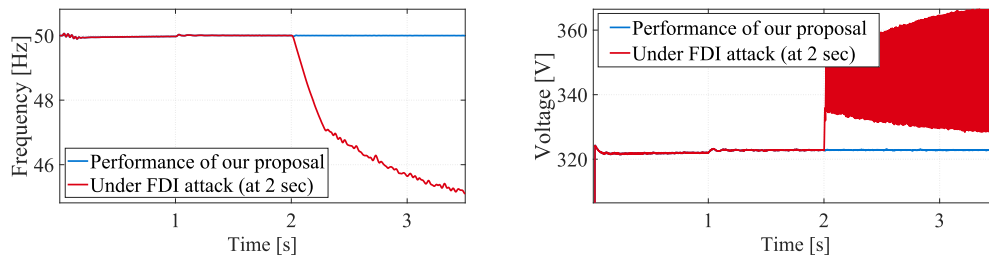


**FIGURE 15.** Frequency and voltage with and without the proposed mitigation strategy.

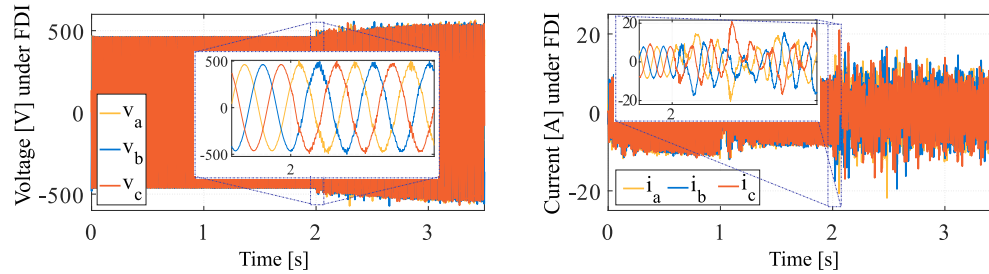


**FIGURE 16.** Voltage and current measured during FDI attacks.

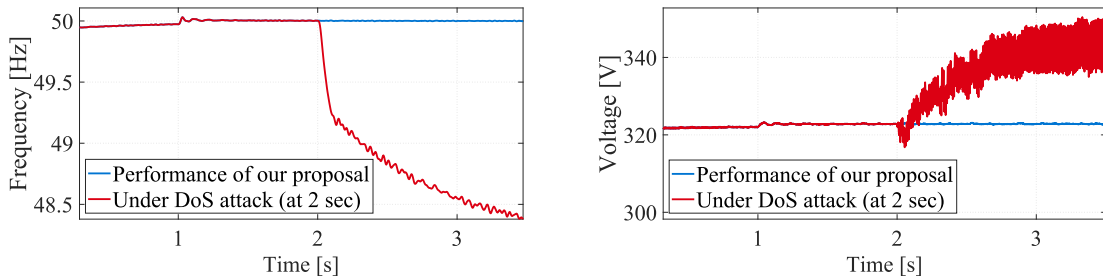


**FIGURE 17.** Defense step against DoS attacks on the SDN proposal and without mitigation algorithm.

to indicate that a device needs to migrate to a new host. In this way, if the HTS service receives a message from a new location without first obtaining a *port-down* message from the previous device, the SDN controller will automatically block traffic from that host and the port will become unavailable. Even if the MAC or IPs are spoofed, the attacking host will be isolated from the rest of the system.

An algorithm proposed to avoid the impact of FDI and hijacking attacks is shown on the next page as Algorithm 1. The corresponding Fig. 15 and Fig. 16 show the microgrid's performance under an FDI attack, initiated at 2 seconds. As can be seen in those figures, the system behavior without FDI consideration is unacceptable, which is evident from the frequency and voltage collapse.

When applying the proposed algorithm based on SDN, the system performance resembles the behavior of hierarchical control under normal conditions (as shown by blue line in Fig. 15). Small deviations from the setpoint observed in Fig. 15 are due to propagation delay in the control implementation and limitations of the SDN controller processing

capacity. However, these deviations are within the acceptable limits according to IEC 61850.

#### B. MITIGATION OF AVAILABILITY-ORIENTED ATTACKS

A DoS attack aims to overload the communications devices' routing table (or flows). Fig. 14 has previously shown the strategy proposed to mitigate DoS attacks. The input values are the frequency and the voltage that are passed to the secondary control. Additionally, if the total bandwidth utilization (set at 1Gbps as an example) exceeds 85%, the communication speed of each switch is then limited to half the nominal speed until the workload of the switches decreases.

Fig. 17 illustrates the performance of the proposed algorithm under this attack. For comparison, Fig. 18 represents the consequences in terms of voltage and current without the security considerations. It is clear that without the SDN security restrictions the MG is unstable.

When applying the mitigation strategy, the behavior of the network is practically the same as under normal conditions. To summarize, different vulnerabilities have been analyzed

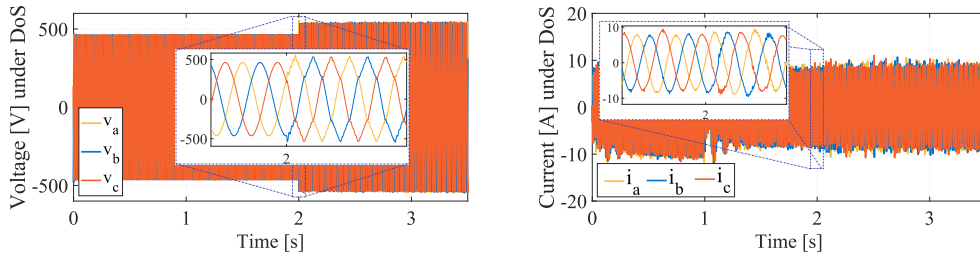


**FIGURE 18.** Voltage and current measured during DoS attacks.

#### Algorithm 1 Proposed Algorithm for FDI Mitigation

```

Input: Frequency and voltage of  $DG_i$  at  $k$ 
Output:  $\delta\omega$  and  $\delta V$  (consensus frequency/voltage)
for  $i$  in normal  $DG$  do
     $S \leftarrow sort(values\ received\ from\ DG_i)$ 
     $N \leftarrow total\ of\ DGs\ in\ S$ 
    if  $DG_i$  value  $\geq S(1)$  then
        | discard the smallest value of  $\omega, V$  received;
    end if
    else if  $DG_i$  value  $\leq S(N)$  then
        | discard the largest value of  $\omega, V$  received;
    end if
    else
        | discards received  $\omega, V$  values farthest from the
        | median of  $S$ ;
    end if
for  $\omega$  and  $V$  in remaining neighbors do
     $\omega(k+1) \leftarrow average\ \omega(N-1);$ 
     $V(k+1) \leftarrow average\ V(N-1);$ 
     $\delta\omega \leftarrow \omega(k+1); \delta V \leftarrow V(k+1);$ 
end for
return  $\delta\omega; \delta V$ 
end for

```

through the integration of virtual machines. Also, security leaks is possible within the GNS3 virtual machine.

## XI. CONCLUSION

This paper has proposed a co-simulation framework for a distributed secondary control strategy to regulate frequency and voltage in a networked MG. The integration of MATLAB/Simulink and GNS3 tools allowed to simulate the electrical system and communications within the same runtime environment. Power sharing in the MG is controlled based on  $P - f$  and  $Q - V$  droop characteristics. The proposed FCS-MPC strategy combined with SDN has been shown to increase the system's reliability and improve power sharing. The paper has demonstrated that the ability to exchange control information between DGs over the SDN network improves the dynamic response of the system to load variations and allows to quickly reach a steady state.

The results presented in this paper have shown that resilience of a power network can be significantly improved by using sophisticated control strategies and programmable communications networks like SDN. Various test scenarios have been proposed in the paper to analyze the performance of the framework, of the control strategies, and the microgrid's behaviour under FDI, DoS and hijacking cyber attacks. The limitations regarding to device data storage in the flow tables that exploit DoS attacks are solved thanks to SDN technology. The proposed framework has been shown to provide a suitable architecture for cybersecurity analysis. The proposed mitigation strategies have improved resilience of the microgrid to cyberattacks by utilizing the benefits of cooperative control strategies.

## REFERENCES

- [1] R. Singh, P. Paniyil, and Z. Zhang, "Transformative role of power electronics: In solving climate emergency," *IEEE Power Electron. Mag.*, vol. 9, no. 2, pp. 39–47, Jun. 2022.
- [2] D. Lew, J. Bakke, A. Bloom, P. Brown, J. Caspary, C. Clack, N. Miller, A. Orths, A. Silverstein, J. Simonelli, and R. Zavadil, "Transmission planning for 100% clean electricity: Enabling clean, affordable, and reliable electricity," *IEEE Power Energy Mag.*, vol. 19, no. 6, pp. 56–66, Nov. 2021.
- [3] N. Hussain, M. Nasir, J. C. Vasquez, and J. M. Guerrero, "Recent developments and challenges on AC microgrids fault detection and protection systems—A review," *Energies*, vol. 13, no. 9, p. 2149, May 2020.
- [4] B. Goutham and H. A. Anoop, "A review on issues, challenges and various optimization techniques in microgrid," *IOP Conf. Ser. Mater. Sci. Eng.*, vol. 937, no. 1, Sep. 2020, Art. no. 012029.
- [5] M. Farrokhabadi, C. A. Cañizares, J. W. Simpson-Porco, E. Nasr, L. Fan, P. A. Mendoza-Araya, and R. Tonkoski, "Microgrid stability definitions, analysis, and examples," *IEEE Trans. Power Syst.*, vol. 35, no. 1, pp. 13–29, Jan. 2019.
- [6] J. B. Almada, R. P. Leão, R. G. Almeida, and R. F. Sampaio, "Microgrid distributed secondary control and energy management using multi-agent system," *Int. Trans. Electr. Energy Syst.*, vol. 31, Oct. 2021, Art. no. e12886.
- [7] W. Yuan, Y. Wang, D. Liu, F. Deng, and Z. Chen, "Efficiency-prioritized droop control strategy of AC microgrid," *IEEE J. Emerg. Sel. Topics Power Electron.*, vol. 9, no. 3, pp. 2936–2950, Jun. 2021.
- [8] R. E. Perez-Guzman, Y. Salgueiro, M. Rivera, and P. W. Wheeler, "Control strategy and communication architecture for power sharing in microgrids," in *Proc. IEEE Int. Conf. Ind. Technol. (ICIT)*, Feb. 2020, pp. 1167–1172.
- [9] T. Dragičević, "Model predictive control of power converters for robust and fast operation of AC microgrids," *IEEE Trans. Power Electron.*, vol. 33, no. 7, pp. 6304–6317, Jul. 2017.
- [10] T. Chen, O. Abdel-Rahim, F. Peng, and H. Wang, "An improved finite control set-MPC-based power sharing control strategy for islanded AC microgrids," *IEEE Access*, vol. 8, pp. 52676–52686, 2020.

- [11] S. Weng, Y. Xue, J. Luo, and Y. Li, "Distributed secondary control for islanded microgrids cluster based on hybrid-triggered mechanisms," *Processes*, vol. 8, no. 3, p. 370, Mar. 2020.
- [12] Y. Zhang and W. Wei, "Decentralised coordination control strategy of the PV generator, storage battery and hydrogen production unit in islanded AC microgrid," *IET Renew. Power Gener.*, vol. 14, no. 6, pp. 1053–1062, Apr. 2020.
- [13] S. Zuo, O. A. Beg, F. L. Lewis, and A. Davoudi, "Resilient networked AC microgrids under unbounded cyber attacks," *IEEE Trans. Smart Grid*, vol. 11, no. 5, pp. 3785–3794, Sep. 2020.
- [14] J. Lai, X. Lu, X. Yu, and A. Monti, "Stochastic distributed secondary control for AC microgrids via event-triggered communication," *IEEE Trans. Smart Grid*, vol. 11, no. 4, pp. 2746–2759, Jul. 2020.
- [15] M. Azeroual, T. Lamhamdi, H. E. Moussaoui, and H. El Markhi, "Simulation tools for a smart grid and energy management for microgrid with wind power using multi-agent system," *Wind Eng.*, vol. 44, no. 6, pp. 661–672, Dec. 2020.
- [16] P. Zhang, *Networked Microgrids*. Cambridge, U.K.: Cambridge Univ. Press, 2021.
- [17] Q. Zhou, M. Shahidehpour, A. Paaso, S. Bahramirad, A. Alabdulwahab, and A. Abusorrah, "Distributed control and communication strategies in networked microgrids," *IEEE Commun. Surveys Tuts.*, vol. 22, no. 4, pp. 2586–2633, 4th Quart., 2020.
- [18] W. Li, M. Ferdowsi, M. Stevic, A. Monti, and F. Ponci, "Cosimulation for smart grid communications," *IEEE Trans. Ind. Informat.*, vol. 10, no. 4, pp. 2374–2384, Nov. 2014.
- [19] V. Kounev, D. Tipper, M. Levesque, B. M. Grainger, T. Mcdermott, and G. F. Reed, "A microgrid co-simulation framework," in *Proc. Workshop Modeling Simulation Cyber-Phys. Energy Syst. (MSCPES)*, Apr. 2015, pp. 1–6.
- [20] V. Kounev, D. Tipper, A. A. Yavuz, B. M. Grainger, and G. F. Reed, "A secure communication architecture for distributed microgrid control," *IEEE Trans. Smart Grid*, vol. 6, no. 5, pp. 2484–2492, Sep. 2015.
- [21] D. Bian, M. Kuzlu, M. Pipattanasomporn, S. Rahman, and Y. Wu, "Real-time co-simulation platform using OPAL-RT and OPNET for analyzing smart grid performance," in *Proc. IEEE Power Energy Soc. Gen. Meeting*, Jul. 2015, pp. 1–5.
- [22] M. Manbachi, A. Sadu, H. Farhangi, A. Monti, A. Palizban, F. Ponci, and S. Arzanpour, "Real-time co-simulation platform for smart grid volt-VAR optimization using IEC 61850," *IEEE Trans. Ind. Informat.*, vol. 12, no. 4, pp. 1392–1402, Aug. 2016.
- [23] V. Venkataramanan, A. Srivastava, and A. Hahn, "Real-time co-simulation testbed for microgrid cyber-physical analysis," in *Proc. Workshop Modeling Simulation Cyber-Phys. Energy Syst. (MSCPES)*, Apr. 2016, pp. 1–6.
- [24] K. Vatanparvar and M. A. A. Faruque, "Application-specific residential microgrid design methodology," *ACM Trans. Design Autom. Electron. Syst.*, vol. 22, no. 3, pp. 1–21, May 2017.
- [25] X. Li, Q. Huang, and D. Wu, "Distributed large-scale co-simulation for IoT-aided smart grid control," *IEEE Access*, vol. 5, pp. 19951–19960, 2017.
- [26] S. Vogel, V. S. Rajkumar, H. T. Nguyen, M. Stevic, R. Bhandia, K. Heussen, P. Palensky, and A. Monti, "Improvements to the co-simulation interface for geographically distributed real-time simulation," in *Proc. 45th Annu. Conf. IEEE Ind. Electron. Soc.*, vol. 1, Oct. 2019, pp. 6655–6662.
- [27] H. F. Habib, M. M. Esfahani, and O. A. Mohammed, "Investigation of protection strategy for microgrid system using lithium-ion battery during islanding," *IEEE Trans. Ind. Appl.*, vol. 55, no. 4, pp. 3411–3420, Jul. 2019.
- [28] N. España, J. Barco-Jiménez, A. Pantoja, and N. Quijano, "Distributed population dynamics for active and reactive power dispatch in islanded microgrids," *Int. J. Electr. Power Energy Syst.*, vol. 125, Feb. 2021, Art. no. 106407.
- [29] Y. C. C. Wong, C. S. Lim, H. H. Goh, A. Cruden, M. D. Rotaru, and X. Kong, "An optimal secondary multi-bus voltage and reactive power sharing control based on non-iterative decoupled linearized power flow for islanded microgrids," *IEEE Access*, vol. 9, pp. 105242–105254, 2021.
- [30] B. Sinkovics, J. Kiss, B. Polgári, and J. Csatár, "Co-simulation framework for calculating balancing energy needs of a microgrid with renewable energy penetration," *Int. J. Energy Res.*, vol. 45, no. 13, pp. 18631–18643, Oct. 2021.
- [31] B. Bhattacharai, L. Marinovic, M. Touhiduzzaman, F. K. Tuffner, K. P. Schneider, J. Xie, P. Thekkumparambath Mana, W. Du, and A. Fisher, "Studying impacts of communication system performance on dynamic stability of networked microgrid," *IET Smart Grid*, vol. 3, no. 5, pp. 667–676, Oct. 2020.
- [32] Z. Wang, D. Qi, J. Mei, Z. Li, K. Wan, and J. Zhang, "Real-time controller hardware-in-the-loop co-simulation testbed for cooperative control strategy for cyber-physical power system," *Global Energy Interconnection*, vol. 4, no. 2, pp. 214–224, Apr. 2021.
- [33] K. Gupta, S. Sahoo, B. K. Panigrahi, F. Blaabjerg, and P. Popovski, "On the assessment of cyber risks and attack surfaces in a real-time co-simulation cybersecurity testbed for inverter-based microgrids," *Energies*, vol. 14, no. 16, p. 4941, Aug. 2021.
- [34] M. Mukherjee, T. Hardy, J. C. Fuller, and A. Bose, "Implementing multi-settlement decentralized electricity market design for transactive communities with imperfect communication," *Appl. Energy*, vol. 306, Jan. 2022, Art. no. 117979.
- [35] Y. Wu, L. Fu, F. Ma, and X. Hao, "Cyber-physical co-simulation of shipboard integrated power system based on optimized event-driven synchronization," *Electronics*, vol. 9, no. 3, p. 540, Mar. 2020.
- [36] R. Heydari, T. Dragicevic, and F. Blaabjerg, "High-bandwidth secondary voltage and frequency control of VSC-based AC microgrid," *IEEE Trans. Power Electron.*, vol. 34, no. 11, pp. 11320–11331, Nov. 2019.
- [37] J. W. Simpson-Porco, Q. Shafiee, F. Dörfler, J. C. Vasquez, J. M. Guerrero, and F. Bullo, "Secondary frequency and voltage control of islanded microgrids via distributed averaging," *IEEE Trans. Ind. Electron.*, vol. 62, no. 11, pp. 7025–7038, Nov. 2015.
- [38] F. Nejabatkhah, Y. W. Li, H. Liang, and R. Reza Ahrabi, "Cyber-security of smart microgrids: A survey," *Energies*, vol. 14, no. 1, p. 27, Dec. 2020.
- [39] Z. Tang, P. Zhang, and W. O. Krawec, "A quantum leap in microgrids security: The prospects of quantum-secure microgrids," *IEEE Electric Mag.*, vol. 9, no. 1, pp. 66–73, Mar. 2021.
- [40] J. A. Villanueva-Rosario, F. Santos-García, M. E. Aybar-Mejía, P. Mendoza-Araya, and A. Molina-García, "Coordinated ancillary services, market participation and communication of multi-microgrids: A review," *Appl. Energy*, vol. 308, Feb. 2022, Art. no. 118332.
- [41] J. R. López Gutiérrez, P. Ponce, and A. Molina, "Real-time power electronics laboratory to strengthen distance learning engineering education on smart grids and microgrids," *Future Internet*, vol. 13, no. 9, p. 237, Sep. 2021.
- [42] E. Rute-Luengo, A. Navas-Fonseca, J. S. Gomez, E. Espina, C. Burgos-Mellado, D. Saez, M. Sumner, and D. Munoz-Carpintero, "Distributed model-based predictive secondary control for hybrid AC/DC microgrids," *IEEE J. Emerg. Sel. Topics Power Electron.*, early access, Mar. 8, 2022, doi: 10.1109/JESTPE.2022.3157979.
- [43] J. S. Gomez, D. Saez, J. W. Simpson-Porco, and R. Cardenas, "Distributed predictive control for frequency and voltage regulation in microgrids," *IEEE Trans. Smart Grid*, vol. 11, no. 2, pp. 1319–1329, Mar. 2020.
- [44] R. E. Perez-Guzman, M. Rivera, N. Vicencio, and P. W. Wheeler, "Model-based predictive control in three-phase inverters," in *Proc. IEEE Int. Conf. Ind. Technol. (ICIT)*, Feb. 2020, pp. 499–504.
- [45] J. Grossmann, *Graphical Network Simulator—3*. Accessed: Jun. 16, 2022. [Online]. Available: <https://gns3.com/software>
- [46] J. Grossmann, *Dynamips (Cisco Router Emulator)*. Accessed: Jun. 16, 2022. [Online]. Available: <https://github.com/GNS3/dynamips>
- [47] (Apr. 30, 2021). *Mininet—An Instant Virtual Network on Your Laptop (or Other PC)*. Accessed: Jun. 16, 2022. [Online]. Available: <http://mininet.org/>
- [48] (May 30, 2021). *Docker Container Hosting Opendaylight-0.3.4-Lithium and Ciscodevnet Opendaylight-Openflow-App*. Accessed: Jun. 16, 2022. [Online]. Available: <https://hub.docker.com/r/ibrm/odlofmngns3>
- [49] X. Hoa Thi Pham, "Power sharing strategy in islanded microgrids using improved droop control," *Electric Power Syst. Res.*, vol. 180, Mar. 2020, Art. no. 106164.
- [50] Linux Foundation. (2022). *OpenDaylight Project, Version 16.0 Sulfur, San Francisco, CA, USA*. [Online]. Available: <https://www.opendaylight.org/>
- [51] N. Singh, I. Elamvazuthi, P. Nallagownden, G. Ramasamy, and A. Jangra, "Routing based multi-agent system for network reliability in the smart microgrid," *Sensors*, vol. 20, no. 10, p. 2992, May 2020.
- [52] C. Powell, C. Desimiotis, and B. Dezfooli, "The fog development kit: A platform for the development and management of fog systems," *IEEE Internet Things J.*, vol. 7, no. 4, pp. 3198–3213, Apr. 2020.

- [53] T. C. Aysal, M. E. Yildiz, A. D. Sarwate, and A. Scaglione, "Broadcast gossip algorithms for consensus," *IEEE Trans. Signal Process.*, vol. 57, no. 7, pp. 2748–2761, Jul. 2009.
- [54] S. Kouachi, S. Dhuli, and Y. N. Singh, "Convergence rate analysis of periodic gossip algorithms for one-dimensional lattice WSNs," *IEEE Sensors J.*, vol. 20, no. 21, pp. 13150–13160, Nov. 2020.
- [55] Q. Shafiee, Č. Stefanović, T. Dragičević, P. Popovski, J. C. Vasquez, and J. M. Guerrero, "Robust networked control scheme for distributed secondary control of islanded microgrids," *IEEE Trans. Ind. Electron.*, vol. 61, no. 10, pp. 5363–5374, Oct. 2014.
- [56] Y. Khayat, Q. Shafiee, R. Heydari, M. Naderi, T. Dragicevic, J. W. Simpson-Porco, F. Dorfler, M. Fathi, F. Blaabjerg, J. M. Guerrero, and H. Bevrani, "On the secondary control architectures of AC microgrids: An overview," *IEEE Trans. Power Electron.*, vol. 35, no. 6, pp. 6482–6500, Jun. 2020.
- [57] A. B. Holvik, "Virtual impedance techniques for power sharing control in AC islanded microgrids," M.S. thesis, Dept. Electr. Power Eng., NTNU, Trondheim, Norway, 2018.
- [58] J. Fang, H. Li, Y. Tang, and F. Blaabjerg, "On the inertia of future more-electronics power systems," *IEEE J. Emerg. Sel. Topics Power Electron.*, vol. 7, no. 4, pp. 2130–2146, Dec. 2019.
- [59] Y. Li, P. Zhang, and M. Yue, "Networked microgrid stability through distributed formal analysis," *Appl. Energy*, vol. 228, pp. 279–288, Oct. 2018.
- [60] M. Azab, "Comparative study of BLDC motor drives with different approaches: FCS-model predictive control and hysteresis current control," *World Electr. Vehicle J.*, vol. 13, no. 7, p. 112, Jun. 2022.
- [61] K. Singh, M. Amir, F. Ahmad, and M. A. Khan, "An integral tilt derivative control strategy for frequency control in multimicrogrid system," *IEEE Syst. J.*, vol. 15, no. 1, pp. 1477–1488, Mar. 2021.
- [62] K. Singh, M. Amir, F. Ahmad, and S. S. Refaat, "Enhancement of frequency control for stand-alone multi-microgrids," *IEEE Access*, vol. 9, pp. 79128–79142, 2021.
- [63] K. Singh and M. Amir, "Intelligent fuzzy TIDF-II controller for load frequency control in hybrid energy system," *IETE Tech. Rev.*, vol. 2021, pp. 1–17, Nov. 2021.
- [64] R. E. Pérez-Guzmán, Y. Salgueiro-Sicilia, and M. Rivera, "Communications in smart grids," in *Proc. IEEE CHILEAN Conf. Elect., Electron. Eng., Inf. Commun. Technol. (CHILECON)*, Jan. 2017, pp. 1–7.
- [65] H. Zhang, W. Meng, J. Qi, X. Wang, and W. X. Zheng, "False data injection attacks on inverter-based microgrid in autonomous mode," in *Distributed Control Methods and Cyber Security Issues in Microgrids*. Amsterdam, The Netherlands: Elsevier, 2020, pp. 125–146.
- [66] N. Priyadarshini, S. Gomathy, and M. Sabarimuthu, "A review on microgrid architecture, cyber security threats and standards," *Mater. Today, Proc.*, vol. 2020, pp. 1–15, Dec. 2020.
- [67] S. Marchand, C. Monsalve, T. Reimann, W. Heckmann, J. Ungerland, H. Lauer, S. Ruhe, and C. Krauß, "Microgrid systems: Towards a technical performance assessment frame," *Energies*, vol. 14, no. 8, p. 2161, Apr. 2021.
- [68] Q. Zhou, M. Shahidehpour, A. Alabdulwahab, A. Abusorrah, L. Che, and X. Liu, "Cross-layer distributed control strategy for cyber resilient microgrids," *IEEE Trans. Smart Grid*, vol. 12, no. 5, pp. 3705–3717, Sep. 2021.
- [69] Q. Zhou, M. Shahidehpour, A. Alabdulwahab, and A. Abusorrah, "A cyber-attack resilient distributed control strategy in islanded microgrids," *IEEE Trans. Smart Grid*, vol. 11, no. 5, pp. 3690–3701, Sep. 2020.
- [70] S. Sahoo and J. C.-H. Peng, "A localized event-driven resilient mechanism for cooperative microgrid against data integrity attacks," *IEEE Trans. Cybern.*, vol. 51, no. 7, pp. 3687–3698, Jul. 2021.
- [71] P. Braun, L. Grüne, and C. M. Kellett, *(In-)Stability of Differential Inclusions: Notions, Equivalences, and Lyapunov-Like Characterizations*. Cham, Switzerland: Springer, 2021.
- [72] X. Li, Z. Li, L. Guo, J. Zhu, Y. Wang, and C. Wang, "Enhanced dynamic stability control for low-inertia hybrid AC/DC microgrid with distributed energy storage systems," *IEEE Access*, vol. 7, pp. 91234–91242, 2019.
- [73] Y. Li, Y. Qin, P. Zhang, and A. Herzberg, "SDN-enabled cyber-physical security in networked microgrids," *IEEE Trans. Sustain. Energy*, vol. 10, no. 3, pp. 1613–1622, Jul. 2019.
- [74] Z. Jiang, Z. Tang, P. Zhang, and Y. Qin, "Programmable adaptive security scanning for networked microgrids," *Engineering*, vol. 7, no. 8, pp. 1087–1100, Aug. 2021.
- [75] N. Yassaie, M. Hallajian, I. Sharifi, and H. A. Talebi, "Resilient control of multi-microgrids against false data injection attack," *ISA Trans.*, vol. 110, pp. 238–246, Apr. 2021.
- [76] Z. Shahbazi, A. Ahmadi, A. Karimi, and Q. Shafiee, "Performance and vulnerability of distributed secondary control of AC microgrids under cyber-attack," in *Proc. 7th Int. Conf. Control, Instrum. Autom. (ICCIA)*, Feb. 2021, pp. 1–6.
- [77] S. Ma, Y. Li, L. Du, J. Wu, Y. Zhou, Y. Zhang, and T. Xu, "Programmable intrusion detection for distributed energy resources in cyber-physical networked microgrids," *Appl. Energy*, vol. 306, Jan. 2022, Art. no. 118056.
- [78] Q. Li, A. Li, T. Wang, and Y. Cai, "Interconnected hybrid AC–DC microgrids security enhancement using blockchain technology considering uncertainty," *Int. J. Electr. Power Energy Syst.*, vol. 133, Dec. 2021, Art. no. 107324.
- [79] M. Ghiasi, M. Dehghani, T. Niknam, A. Kavousi-Fard, P. Siano, and H. H. Alhelou, "Cyber-attack detection and cyber-security enhancement in smart DC-microgrid based on blockchain technology and Hilbert Huang transform," *IEEE Access*, vol. 9, pp. 29429–29440, 2021.



**RICARDO E. PÉREZ GUZMÁN** (Member, IEEE) received the B.S. degree in telecommunications and electronics engineer from Oriente University, Cuba, in 2011, and the M.S. degree from the Department of Computer Science, Las Tunas University in Informatics Applied, in 2015. He is currently pursuing the Ph.D. degree in engineering systems with the University of Talca, Chile. Since 2018, he has been working as a Professor with the Computer Science Department, University of Talca. His research interests include communication, intelligent energy systems, predictive control, and distributed control.



**MARCO RIVERA** (Senior Member, IEEE) received the degree in electronic civil engineering and the M.Sc. degree in engineering with specialization in electrical engineering from the Universidad de Concepción, and the Ph.D. degree in electronic engineering from the Universidad Técnica Federico Santa María.

He has directed and participated in several projects financed by the National Fund for Scientific and Technological Development (Fondo Nacional de Desarrollo Científico y Tecnológico, FONDECYT), the National Commission for Scientific and Technological Research (Comisión Nacional de Investigación Científica y Tecnológica, CONICYT), and the Paraguayan Program for the Development of Science and Technology (Proyecto Paraguayo para el Desarrollo de la Ciencia y Tecnología, PRO-CIENCIA), among others. He has been the responsible researcher of basal financed projects whose objective is to enhance, through substantial and long-term financing, Chile's economic development through excellence and applied research. He has managed several bilateral agreements for the Universidad de Talca with international universities. He is currently the Director of the Laboratory of Energy Conversion and Power Electronics (Laboratorio de Conversión de Energías y Electrónica de Potencia, LCEEP) and the Technology Center for Energy Conversion (Centro Tecnológico de Conversión de Energía, CTCE). He is also a Full Professor with the Department of Electrical Engineering from the Universidad de Talca. His main research interests include matrix converters, predictive and digital controls for high-power drives, four-leg converters, development of high-performance control platforms based on field-programmable gate arrays, renewable energies, advanced control of power converters, design, assembly, and start-up of power converters. He was awarded with the Premio Tesis de Doctorado Academia Chilena de Ciencias 2012, for the Best Ph.D. thesis developed in 2011 for national and foreign students in any exact or natural sciences program, that is a member of the Academia Chilena de Ciencias, Chile. Through the last years, he has been a visiting professor at several international universities.



**PATRICK W. WHEELER** (Fellow, IEEE) received the B.Eng. degree (Hons.) from the University of Bristol, U.K., in 1990, the Ph.D. degree in electrical engineering for his work on matrix converters from the University of Bristol, in 1994. In 1993, he moved to the University of Nottingham, U.K., worked as a Research Assistant at the Department of Electrical and Electronic Engineering. In 1996, he became a Lecturer at the Power Electronics, Machines and Control Group, University of Nottingham, where he has been a Full Professor, since January 2008. He was the Head of the Department of Electrical and Electronic Engineering at the University of Nottingham, from 2015 to 2018. He is currently the Head of the Power Electronics, Machines and Control Research Group, Global Director of the University of Nottingham's Institute of Aerospace Technology, and was the Li Dak Sum Chair Professor in electrical and aerospace engineering. He has published over 750 academic publications in leading international conferences and journals. He is a member of the IEEE PELs AdCom and IEEE PELS Vice-President for technical operations.



**EDUARDO E. ESPINOSA** (Member, IEEE) was born in Concepción, Chile, in 1983. He received the Engineering degree in electronic engineering, in 2009, and the D.Sc. degree in electrical engineering from the University of Concepción, Concepción, in 2015, with a scholarship from the Chilean Research Fund ANID. Since August 2014, he has been with the Department of Electrical Engineering, Universidad Católica de la Santísima Concepción, Concepción, where he is currently an Assistant Professor in teaching and researching the power electronics and control systems. Since January 2022, he is the Program Director of the master's degree in energy systems. His research interests include predictive model control in power converters, multilevel converters, efficiency in power converters, and minimization of THD in multicell power converters.



**GALINA MIRZAEVA** (Senior Member, IEEE) received the B.Eng. degree in electronic engineering and the Ph.D. degree in electrical engineering from the South Urals State University, Russia, in 1990 and 1997, respectively. From 2004 to 2010, she was a Senior Researcher with CRC-Mining, Australia. Since 2010, she has been with the School of Electrical Engineering and Computing, University of Newcastle, Australia, first as a Senior Lecturer, and since 2017, has been an Associate Professor. Her research interests include electric machines and drives, power electronics, and renewable energy applications. From 2009 to 2011 and since 2020, she has been served as the Chair of the IEEE IAS Mining Industry Committee.



**JAIME A. ROHTEN** (Senior Member, IEEE) received the Engineering degree (Hons.) in electronic engineering and the M.Sc. and D.Sc. degrees in electrical engineering from the University of Concepcion, Concepcion, Chile, in 2010, 2012, and 2017, respectively. His research interests include renewable energies, digital nonlinear, resonant, and predictive control for voltage or current source converters. Since 2015, he has been teaching in the areas of power electronic and control systems analysis with the Department of Electrical and Electronic Engineering, Universidad del Bío-Bío, Concepción.

• • •